THERMOGRAVIMETRIC STUDY ON THE PYROLYSIS KINETIC MECHANISM OF WASTE BIOMASS FROM FRUIT PROCESSING INDUSTRY

by

Bojan Ž. JANKOVIĆ[a], Miloš B. RADOJEVIĆ[b], Martina M. BALAĆ[c], Dragoslava D. STOJILJKOVIĆ[b*], and Nebojša G. MANIĆ[b]

[a] Department of Physical Chemistry, Vinča Institute of Nuclear Sciences, University of Belgrade, Belgrade, Serbia
[b] Fuel and Combustion Laboratory, Faculty of Mechanical Engineering, University of Belgrade, Belgrade, Serbia
[c] Department of Process Engineering and Environment Protection, Faculty of Mechanical Engineering, University of Belgrade, Belgrade, Serbia

Original scientific paper
https://doi.org/10.2298/TSCI200213191J

The detailed kinetic analysis of slow pyrolysis process of apricot (Prunus armeniaca L.) kernal shells has been estimated, under non-isothermal conditions, through thermogravimetric analysis and derivative thermogravimetry. Thermal decomposition was implemented using four different heating rates (5, 10, 15, and 20 °C per minute), with consideration of how this parameter effects on the process kinetics. The higher heating rates provoke the shift of thermoanalytical curves towards more elevated temperatures. Using isoconversional differential method, the variation of activation energy, E_a, with conversion fraction, α, was detected, and pyrolysis reaction profile was discussed. After resolving the pyrolysis rate curves of individual biomass constituents, the temperature and conversion ranges of their thermal transformations were clearly identified. In the latter stage of analysis, every identified reaction step was considered through mechanistic description, which involves selection of the appropriate kinetic model function. The comparison of the results as well as discrepancies between them has been discussed. The corresponding rate-law equations related to thermal decomposition reactions of all biomass constituents present in the tested agricultural waste material have been identified.

Key words: *agricultural waste biomass, pyrolysis kinetics, master-plots method, secondary lignin decomposition, dehydroxylation*

Introduction

Gasification and pyrolysis are thermochemical processes of biomass decomposition which were very intricate, since they are influenced by several operative conditions [1]. Among these ones, there is the temperature at which the process is implemented, the process heating rate, as well as the duration of the treatment. Both, the yields of the process products and their qualitative characteristics are the results which were very influenced by the afore-listed parameters.

* Corresponding author, e-mail: dstojiljkovic@mas.bg.ac.rs

In comparison with fast pyrolysis, the slow pyrolysis process is carried out using very low heating rates, and long-lasting treatments, with the aim to maximize the char yield. A correct planning of the biomass treatment requires an accurate evaluation of the process constant rate. Moreover, the entropy production during such process allows determining the environmental impact index [2].

The thermogravimetric analysis (TGA) allows estimating the volatilization kinetic parameters of the slow pyrolysis such as the pre-exponential (frequency) factor, A, and the activation energy, E_a, that characterizes the mathematical expression of the Arrhenius kinetic law equation. This experimental and analytical procedure is very frequently utilized in the studies concerning wood carbonization and thermal decomposition of solid components among these represents the biomass feedstock [3-7].

The kinetic parameters, calculated by isothermal models, even if less reliable, are characterized by the advantage to be not influenced by the specific mathematical model used [8]. Isoconversional models or free models are denominated in this way since they hypothesize constant the conversion degree of biomass and, hence, the constant rate only function by the process temperature. Thanks to these hypotheses it is possible to avoid of arbitrarily supposing the mathematical expression of the constant rate, without knowing the real chemical mechanism of thermal volatilization of biomass [9]. The spread of differential methods was aided by the recent advancements in the branch of the mathematical functions able to fit conspicuous series of experimental data [10]. The differential free model of the Friedman [11] is the quite wide-spread in the literature studies for calculating the kinetic terms of the mathematical expression of Arrhenius kinetic law equation [12].

In this research, we discussed the kinetic behavior of agricultural biomass waste during slow pyrolysis process such as the apricot kernel shells (AKS), where the kinetic parameters together with reaction mechanism were estimated, from the multiple TGA measurements under non-isothermal conditions. It was applied the Friedman method to fit the experimental data of the TGA. The established results were used for determination of mechanism functions that describe decomposition processes of each individual constituent of biomass (hemicelluloses, cellulose and lignin) through application of master-plot method [13]. The Friedman differential method was applied, among the ones available in scientific literature, since it does not overrate the kinetic parameters in comparison with the integral models. Moreover, the method was selected for its trustworthiness in the examined conversion range (sufficiently distant from the initial and the final instants of the biomass decomposition). Finally, the Friedman differential method is a very trustworthy method among the isoconversional ones. This study provides useful information for the implementation of kinetic mathematical models with the aim to optimize the pyrolysis process efficiency.

Moreover, the investigated biomass (AKS) is very important in the Republic of Serbia. However, modern intensive apricot production is highly dependent on environmental conditions. Fruit growing is one of the very important agricultural branches represented in the Republic of Serbia. Apricot (*Prunus armeniaca* L. or *Armeniaca vulgaris* L.) originates from northeastern China, from where it has spread further into the world. Apricot trees mature after 3-4 years and regularly give birth on carefully selected grounds. It is more resistant to plant diseases and pests than most other fruit species, so protection is less expensive. For information, in Serbia, there are about 5290 hectares under apricot plantings. The amount of annual production in recent years varies from 18510 tons in 2005 to 44077 tons in 2011, with average production over the past five years at 26510 tones. Part of this production was addressed to the factories, which also produce tons of residuals of apricot, such as pits, stones or shells which

could be estimated up to 10% of fruit production, respectively between 2500-3000 tons per year [14].

Experimental

Material and sample preparations

The sample preparation of apricot (*Prunus armeniaca* L.) kernel shells as a waste from food industry was done according to standard procedure in order to reach moisture equilibrium and reduce size and to obtain analytical sample. The obtained particle size reduced sample, milled sample is passed through a sieve with a hole size of $d_p \sim 1$ mm (~ 1000 μm), was used for data determination in ultimate and proximate analyses in accordance with appropriate standards [15, 16].

Thermal analysis measurements

The NETZSCH STA (simultaneous thermal analysis) 445 F5 Jupiter system, was used for thermoanalytical (TA) measurements of powdered biomass samples. The sample mass used in the experiments was about 5.0 ± 0.3 mg. The small sample mass was used to avoid resistance of probable effect of the mass and heat transfer during the process of biomass decomposition. The temperature range which is operated during experiments was between room temperature (RT) and 900 °C. The slow pyrolysis was performed in alumina crucibles able to contain small sample masses, using argon (Ar) as the carrier gas, with the total gas-flow rate of 30 mL per minute. The decomposition process was monitored at several heating rates of 5, 10, 15, and 20 °C per minute.

The derivative thermogravimetry (DTG) plots have been built from the experimental TGA values. In order to obtain the reliable DTG curves, it was necessary to apply an analytical procedure, before of carrying on the mathematical differentiation of the TGA data. With the aim to reduce the noise in the TGA, the *moving average* procedure was applied to smooth out irregularities (peaks and valleys) in the experimental data and to easily recognize their trends. This procedure was conducted with assistance of Proteus® operating tools program, already incorporated within NETZSCH STA 445 F5 Jupiter device system.

Every measurement was repeated twice for checking the reproducibility of thermal analysis tests, where all tests are showed satisfactory reproducibility of TA data. Such procedure allowed the considerable improvement of the TGA data and, consequently, allowed of obtaining trustworthy and accurate results through the successive mathematical fitting.

Kinetic analysis

Friedman isoconversional differential method

The kinetic models are built on a mathematical expression which links the constant rate, $k(T)$, even named *the reaction rate*, to the process temperature. The Arrhenius mathematical expression describes this link and it can be described by:

$$k(T) = A\exp\left(-\frac{E_a}{\mathrm{R}T}\right) \tag{1}$$

where $k(T)$ [min^{-1}] is temperature-dependent rate constant, A [min^{-1}] – the pre-exponential factor, E_a [Jmol^{-1}] – the activation energy, R [= 8.314 Jmol^{-1}K^{-1}] – the gas constant, and T [K] – the absolute temperature. The exponential part, in the eq. (1), indicates the molecular impacts which have a level of kinetic energy capable to provoke the chemical reaction. Even if the pre-exponential factor is lightly influenced by T, the part mainly influenced by T in eq. (1),

is the exponential one. The biomass thermal volatilization can be kinetically described by the following equation [17]:

$$\frac{\mathrm{d}\alpha}{\mathrm{d}t} = k(T)f(\alpha) = A\exp\left(\frac{E_a}{\mathrm{R}T}\right)f(\alpha) \tag{2}$$

where the $\mathrm{d}\alpha/\mathrm{d}t$ [min^{-1}] is the overall process rate, t – the time, and $f(\alpha)$ – the mathematical function which expresses the decomposition of biomass sample. This function is strongly linked to the particular mechanism of devolatilization, which was supposed. The term α represents the degree of conversion of biomass (or the conversion fraction), which is dimensionless ($\alpha \sim$ 0-1). This last one can be expressed by the formula: $\alpha = (m_\mathrm{o} - m_T)/(m_\mathrm{o} - m_f)$, where m_o is the initial biomass sample, m_T is the current biomass sample at arbitrary temperature T, and at the time t, and m_f is the final (equilibrium at $t \to \infty$) biomass sample at the end of process measurement, respectively. Under the linear program of the sample heating and non-isothermal ($\beta = \mathrm{d}T/\mathrm{d}t$) conditions, the eq. (2) can be expressed:

$$\beta\left(\frac{\mathrm{d}\alpha}{\mathrm{d}T}\right) = \left(\frac{\mathrm{d}T}{\mathrm{d}t}\right)\left(\frac{\mathrm{d}\alpha}{\mathrm{d}T}\right) \equiv \frac{\mathrm{d}\alpha}{\mathrm{d}t} = A\exp\left(-\frac{E_a}{\mathrm{R}T}\right)f(\alpha) \tag{3}$$

By re-arrangements of the eq. (3) and subsequently integrating, the following equation was obtained:

$$\int_0^\alpha \frac{\mathrm{d}\alpha}{f(\alpha)} \equiv g(\alpha) = \left(\frac{A}{\beta}\right)\int_0^T \exp\left(-\frac{E_a}{\mathrm{R}T}\right)\mathrm{d}T \cong \left(\frac{A}{\beta}\frac{E_a}{\mathrm{R}}\right)\pi\left(\frac{E_a}{\mathrm{R}T}\right) = \left(\frac{AE_a}{\beta\mathrm{R}}\right)\pi(x) \tag{4}$$

where $g(\alpha)$ is the integral form of the mathematical function which describes the mechanism of biomass decomposition (depends on the explicit expression of $f(\alpha)$ function), while $\pi(x)$ ($x = E_a/\mathrm{R}T$ is the reduced activation energy) represents the mathematical approximation of the temperature integral, which stands on the right-hand side of the eq. (4) ($\int\exp(-E_a/\mathrm{R}T)\mathrm{d}T$). The variation of biomass conversion fraction, $\mathrm{d}\alpha$, with the respect to the temperature, T, physically corresponds to the part of biomass that did not convert in volatiles compounds. Considering all available solid-state kinetic models [18], the volumetric model represents the model based on *order of the reaction*, which hypothesizes order of reaction $n = 1$. Since traditionally Friedman's method is based on volumetric model assumption, it was later significantly upgraded to a wider range of solid-state kinetic models [18]. The Friedman method is based on the logarithmic form of the eq. (2), without introducing any approximations for the temperature integral, which apparently exist in the case of isoconversional integral methods, in a form:

$$\ln\left(\beta\frac{\mathrm{d}\alpha}{\mathrm{d}T}\right)_\alpha \equiv \ln\left(\frac{\mathrm{d}\alpha}{\mathrm{d}t}\right)_{\beta,\alpha} = \ln\left[Af(\alpha)\right]_{\beta,\alpha} - \frac{E_{a,\alpha}}{\mathrm{R}T_{\beta,\alpha}} \tag{5}$$

Plotting the left-hand side of eq. (5), $\ln(\mathrm{d}\alpha/\mathrm{d}t)_{\beta,\alpha}$, against $1/T_{\beta,\alpha}$, at the several and constant conversion fraction values (α = constant), it is a possible to obtain a set of straight lines at various conversion fractions (α). The slope of these straight lines is equal to $-E_{a,\alpha}/\mathrm{R}$ and the intercept is equal to $\ln[A{\cdot}f(\alpha)]_{\beta,\alpha}$. Consequently, through the mathematical equation of the straight line, it is feasible to calculate the terms A and $f(\alpha)$.

Reaction mechanism determination

The identification of complex biomass decomposition stages during thermally induced process, the deconvolution method for describing the conversion rate curves was per-

formed and detailed description of this procedure can be found elsewhere [19]. The performed deconvolution procedure allows separation the reaction temperature ranges, where the individual constituent of biomass takes place decomposition reaction, during the entire pyrolysis process. In order to determine the mechanism functions, the master-plot method was used to choose an appropriate kinetic model. Regarding the already published methodology [14], the special function $z(\alpha)$ was used for kinetic modeling of considered reaction step in the pyrolysis mechanism scheme, and can be expressed:

$$z(\alpha) = f(\alpha)g(\alpha) = \left(\frac{\mathrm{d}\alpha}{\mathrm{d}t}\right)_{\alpha} T_{\alpha}^{2}\left[\frac{\pi(x)}{\beta T_{\alpha}}\right] \tag{6}$$

where $g(\alpha)$ is the integral form of the reaction mechanism function, $(\mathrm{d}\alpha/\mathrm{d}t)_{\alpha}$ – the conversion rate at the specific extent of reaction value (the conversion fraction, α), T_{α} – conversion related temperature, β – the considered heating rate, while $\pi(x)$ is the mathematical approximation of the temperature integral. The term $[\pi(x)/\beta T_{\alpha}]$ in the eq. (6) has a negligible effect on the shape of the $z(\alpha)$ function. Thus, the shapes of $z(\alpha)$ can be determined for each value of α by multiplying the experimental values of $(\mathrm{d}\alpha/\mathrm{d}t)_{\alpha}$ and T_{α}^{2}. The resulting experimental values of $z(\alpha)$ are plotted as a function of α and compared against theoretical $z(\alpha)$ master-plots. A suitable model is identified as the best match between the experimental and theoretical $z(\alpha)$ master-plots. From a series of experimental kinetic curves measured at different heating rates, one can obtain a series of the experimental $z(\alpha)$ plots that should, however, yield a single dependence of $z(\alpha)$ on α, which is practically independent of the heating rate. The theoretical $z(\alpha)$ master-plots were obtained by plotting the product of $f(\alpha)g(\alpha)$ against the α, for the different reaction models. The list of reaction models used in this work was provided in [18].

Results and discussion

Ultimate and proximate analysis of raw biomass sample

Table 1 shows comparison between ultimate and proximate analysis results of AKS biomass used in this work with the same analysis related to apricot stone sample reported in [20].

Comparing both, AKS and apricot stones, these samples contain moisture content below 10%, which is adequate for thermochemical process of biomass conversion into the energy. If we consider all presented quantities, apricot stone has higher values than AKS

Table 1. Results of proximate and ultimate analysis of the raw AKS sample compared with ones related to apricot stone samples (*dry basis*) which have been reported in [20]

	AKS (this study)	Apricot stone[b] [20]		AKS (this study)	Apricot stone[b] [20]
	Proximate analysis [wt.%]			Ultimate analysis[b] [wt.%]	
Moisture	9.71	7.76	Carbon	46.88	50.66
VM	73.84	81.85	Hydrogen	6.38	5.45
FC	15.51	17.41	Oxygen[c]	45.45	43.05
Ash	0.94	0.64	Nitrogen	0.25	0.12
HHV [MJkg^{-1}]	20.26	-	Sulphur	0.00	0.08
LHV [MJkg^{-1}][a]	18.72	-			

[a] Calculated according [21].
[b] On a dry basis.
[c] By the difference.

for volatile matter (VM), fixed carbon (FC), carbon contents (C), and sulphur contents (S). Also, the ash content was lowered in comparison with AKS sample, tab. 1. A significant difference occurs in content of hydrogen (H) and oxygen (O) of which there are more in the AKS sample, tab. 1. This suggests that in comparison with apricot stones, the AKS would have produced much better char (solid residue) quality, concerning its porous structure, giving a much higher surface area [22]. This has also been confirmed by works previously reported in [23-25]. Earlier, it was showed that investigation on the composition of the tar obtained by pyrolysis of agricultural biomass waste is pointing that the basic part of the tar is composed of oxygen containing compounds derivatives of phenol, guaiacol, veratrol, syringol, free fatty acids and esters of fatty acids [26]. These structures can take part in the polycondensation processes. This shows that tar is suitable for the production of carbon adsorbents having great amounts of oxygen containing structures. In addition, on the mass and the porous properties of obtained char and subsequently activated carbons derived from lignocellulosic waste materials, the contributions of hemicelluloses, cellulose and lignin are very significant, especially when it comes from lignin, since that the lignin is the major contributor of chars and activated carbons [27]. Considering these facts, AKS is rich with lignin contents compared to apricot stone, and this can be observed from tab. 2. The tab. 2 provides comparison of the results related to chemical component (lignocellulosic) analysis of two waste materials (AKS and apricot stone samples) [28, 29]. Some differences among samples related to lignocellulosic analysis may be explained by the multitude factors, such as differences in apricot species, climatic and geographical conditions, as well as in the experimental methods.

Table 2. Chemical composition and fiber analysis of two waste biomasses: AKS [28] and apricot stones [29]

Biomass waste[a]	AKS (source from [28])	Apricot stone (source from [29])
Hemicelluloses [%]	23.7	28.0
Cellulose [%]	26.5	30.0
Lignin [%]	35.0	25.8
Hollocellulose [%]	50.2	58.0

[a] The moisture, the ash and extractive contents are included in the analysis.

The total fibrious material content (holloceluluse (the total polysaccharide fraction) = hemicelluloses + cellulose) is a little higher in apricot stone sample than in AKS sample. The structure and composition of hemicellulosic polysaccharides differ depending on plant species classification, *i.e.*, taxonomy. In this context, the thermal decomposition rate of the biomass, depending on the lignocellulosic *fraction*, plays an important role for its conversion in valuable added products. For example, the char obtained from cellulose-rich biomass has approximately equal macro- and micro-pore volumes [29]. On the other hand, the char obtained from lignin-rich biomass has a highly developed porous structure, with a prevalence of macro-pores. The macro-pores prevail in the chars obtained from cherry stones, which have also higher content of lignin [29]. In recent reports, it was found that char obtained from AKS is characterized by the various pore sizes (including super micro-pores and meso-pores) structures [23]. The macro-pores are almost missing in the char obtained from apricot stones [29], which have the lower lignin content compared to AKS.

The VM determines the stability and conversion efficiency of biomass derived fuel. The implication of high VM in biomass feedstock is an increased amount of bio-fuel produc-

tion through pyrolysis process. The studied AKS biomass feedstock is characterized by the high VM content, as well as another comparing feedstock, which was listed in tab. 1. Since the VM of biomass is the condensable vapor and permanent gases (exclusive of water vapor) released from biomass when it is heated. The higher VM content may implies the increased amount of bio-oil production through pyrolysis process. However, its amount depends on the heating conditions including the heating rate, temperature, as well as the residence time. From presented results in tab. 1, we can expect that AKS compared to apricot stone would give a smaller percentage of bio-oil. On the other hand, when the pyrolysis takes place at high temperature values, usually it raises HHV value, because of the higher FC content and dropped the VM value. However, this is not the case for the materials presented in tab. 1. Therefore, for our investigated biomass waste material, maintaining the pyrolytic process at lower temperatures is strongly recommended.

Since that the AKS sample was richer in the carbon content, with moisture content higher than 5 wt.% and with higher oxygen content, tab. 1, all of these issues make the observed biomass feedstock to be poorer in the energy content. However, the higher oxygen content is due to the AKS lignocellulosic structure formed by C, O, H, and N bonds that form the hemicelluloses, cellulose, and lignin, being the main components of lignocellulosic biomass. The low energy content of AKS compared to other energy sources, such as natural gas (27.10 MJ/kg) and mineral coal (47.40 MJ/kg) [30], is due to high oxygen content. Since the energy content is related to higher C and H amount, the biomass with the lowest O/C ratio presented the highest HHV values of biomass sample. The HHV value, tab. 1, is the within the HHV values range attributed to agricultural wastes [31]. The high atomic ratios of H/C and O/C reduce the energy value of considered bio-fuel. Figure 1. shows the Van Krevelen diagram that represents the area dependency between H/C and O/C atomic ratios of the various fuels including biomass, together with their positions of the compared waste biomass samples, *i. e.*, AKS and apricot stone feedstock's.

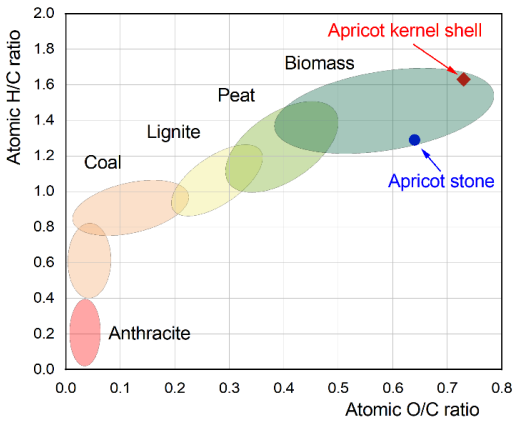

Figure 1. Van Kravelen diagram adapted for the comparative analysis of AKS (this study) (♦) and apricot stones (●) [20]

One of the main differences in characteristics of biomass as compared to coal is that biomass possesses a higher value of H/C ratio, fig. 1. Under the same pyrolysis condition, the hydrogen yield generated from biomass is about 5-16 times as high as that generated from coal [32]. Raw AKS is placed on the diagram, fig. 1, exactly at the position which corresponds to biomass rich with cellulose and lignin contents [33]. With an increasing of pyrolysis temperature, it can be expected that H/C atomic ratio will constantly decline, where the same is valid for O/C atomic ratio. This means that formed chars from raw biomasses are turned into a more carbonaceous nature material at the higher pyrolysis temperatures (shifting will take place up to the down left-side corner of Van Krevelen diagram, where is the position of the coal fuels). This reduction is not unusual, because the obtained chars at higher pyrolysis temperatures formed aromatic structures in order to condense the carbon atoms through the loss of oxygen-containing functional groups. On the other hand, the position of raw AKS sample on

Van Krevelen diagram also corresponds to the raw biomass which was richer with hydrogen (higher H content), where this biomass is very convenient as hydrogen donor in co-pyrolysis with coal. So, our tested biomass sample would be a convenient source for hydrogen transfer reactions. The pyrolysis of coal may be influenced by the presence of hydrogen-rich light molecules (CO, CO_2, H_2, CH_4, H_2O, *etc.*) which are rapidly evolved from biomass at high temperature. These pyrolysis gases may take part in volatile-coal interactions and modify the thermal behavior of coal, especially in the temperature range between 400 and 500 °C, where the coal exists in a plastic state. For example, the co-pyrolysis of coal with AKS biomass, in lower temperature range of approximately between 300 °C and 600 °C, the gas formation rate of hydrogen from biomass pyrolysis can be maintained at a constant value, thus increasing availability of hydrogen around the coal particles. There are external hydrogen donors to interfere with the chain radical processes between the coal and biomass radicals and chemical interactions therefore may be occurred.

The TGA and DTG analysis

The TGA and DTG plots are reported in fig. 2 in function of process temperature, *T,* at various heating rates (β = 5, 10, 15, and 20 °C per minute), for AKS slow pyrolysis process.

From obtained experimental TGA-DTG plots, fig. 2, the first mass loss event occurs between ambient and 120 °C, with mass loss which approximately corresponds to removing of moisture. The second event occurs between approximately 190-290 °C, which is the characteristic for hemicelluloses decomposition, amorphous, and branched polysaccharides composed of many pentoses and hexoses, which degrade prior to cellulose [34].

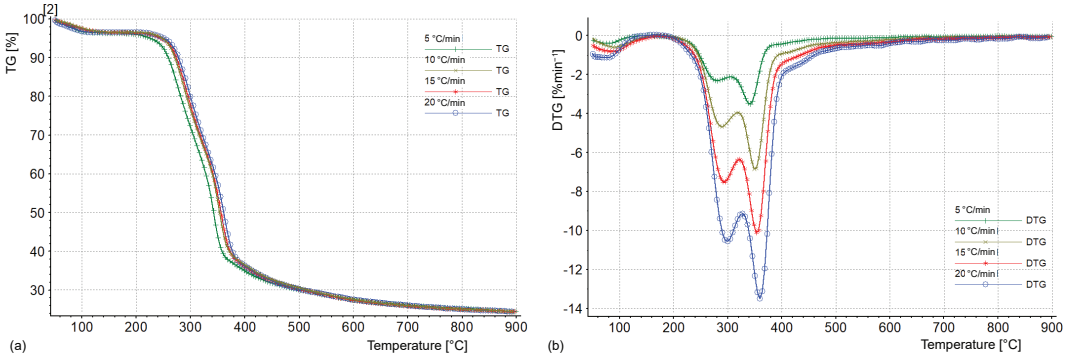

Figure 2. The TGA (a) and DTG (b) plots of AKS slow pyrolysis at various heating rates (5 °C/min, 10 °C/min, 15 °C/min, and 20 °C/min)

The cellulose degrades in a narrow temperature range, because it is a homogeneous semi-crystalline polymer of the glucose units. The cellulose decomposition is prolonged up to approximately 400 °C where the main devolatilization reactions occur, and this represents the *active* pyrolysis stage characterized by the high release of VM. The last event occurs over a wide temperature range from 150 °C to around 900 °C, indicating the lignin decomposition that has a more thermally stable polyaromatic structure and additionally formation of the ash and fixed carbon. The later stage corresponds to the *the passive pyrolysis* process.

Since the mass loss of lignin encompasses wide temperature range with a slower rate, the one DTG profile of can be considered as the overlaps of pseudo components' DTG profiles. Such overlaps give significant hints on the presence of parallel reaction kinetic model,

which pseudo hemicelluloses, cellulose, lignin decompose independently during the pyrolysis process.

It could be observed on the DTG curves at all heating rates, that single small peak occur at around 420 °C and can be attributed to additional lignin decomposing, where the cracking of aromatic rings occurs, where the further goes by breakdowns into the smaller fragments towards the production of bio-oil which consists mainly of alkoxy-phenols and the oxygenated aromatics (*e. g.*, guaiacol, methyl guaiacol, syringol, methyl syringol, vanillin, syringaldehyde, vinyl syringol, vinyl guaiacol, 1, 2, 3-trimethoxy-benzene), as well as some gaseous products (mainly CO_2 and CO) and the char [35, 36].

It was found that occurring of DTG peak nearly 400 °C is a consequence of the produced trace amounts of oxy-aromatics, ketones, furans and alkyl-phenols (not oxygenated) [37]. It has been previously shown that the increase of pyrolysis temperature promotes the decomposition of high molecular weight phenolic oligomers to smaller compounds through the depolymerisation and cracking of C-C bonds [38]. However, the higher temperatures, at least in the range of 450-600 °C, fig. 2, favor formation of low molecular weight species instead of polymerized products and char. At temperatures around 400 °C, relatively larger guaiacol-type compounds may be expected [37], with alkyl side chains as well as oligomers consisting of two coniferyl alcohol units, while by transition to higher temperature zone (around 600 °C), the smaller alkoxy-phenols, *i. e.*, guaiacol, creosol and vanillin can prevail. At that temperature and above, it can be expected that char will decrease as temperature further increased.

Among the numerous operative conditions that significantly affect the thermal decomposition process of biomass, there is the heating rate. It is possible to highlight that the increase of the heating rate produces more accentuated peaks of DTG curves, fig. 2, and that these last ones occur at higher temperatures. Other researchers that carried out the TGA analysis at different heating rate values [39, 40] found similar behavior. The increase of the maximum decomposition rate with the increase of heating rate is related to the very complex structure of the biomass sample, which is composed by a great number of components, each one with a specific peak of decomposition. Namely, when the heating rate is very low, the individual peaks of decomposition produce some *vibrations* in DTG curve. Instead, if heating rate is quite high, since different biomass components volatilize at the same time, the individual peaks of volatilization overlap themselves and cause higher DTG peaks, fig. 2. The effect of heating rate may be specifically pronounced in the case of cellulose thermal decomposition [41]. At low temperatures and low heating rates, strong intra-chain hydrogen bonds of cellulose functional groups, increasing the probability of dehydration reactions. At high heating rates, intra-chain hydrogen bonds weaken and decrease possibility of collisions that facilitate dehydration reactions [42].

Isoconversional analysis of apricot kernel shell slow pyrolysis process

According to the eq. (5), the apparent activation energy values were calculated at different and constant conversion values in the range from $\alpha = 0.04$ to $\alpha = 0.96$, with a conversion step of $\Delta\alpha = 0.02$. Figure 3 shows the isoconversional dependency of the effective activation energy, E_a, on the conversion fraction, α, for slow pyrolysis process of AKS sample. The large identified errors represent the limitation in accuracy consideration of calculated E_a values at very high conversions. Considering this fact, the results obtained from this analysis, fig. 3, suggest that data where the final char is formed (high conversions above $\alpha = 0.82$) is a function of the heating rate, where in that moment the isoconversional principle is violated. Considering the data for $\alpha \geq 0.82$, if the definition of conversion is erroneous, then the isoconversional prin-

ciple will not be satisfied at high conversion values. However, there is no significant influence of $\Delta\alpha$ on derived E_a value for $\Delta\alpha \leq 0.80$.

The shape of the obtained dependency, fig. 3, suggests that the pyrolysis process proceeds through complex reaction mechanism, where slightly increase in E_a value at very low conversions (up to $\alpha \sim 0.10$) can be attributed to dehydration reaction as well as the extractives decomposition at lower temperatures. In another process area, approximately from $\alpha = 0.10$ to $\alpha = 0.40$, fig. 3, the E_a exhibits gradual increase with conversion, from 171.6 kJ/mol to 232.1 kJ/mol which can be attributed to the hemicelluloses decomposition reactions. In the initial stage, the decomposition started easily on weakly linked sites inherent to the polymeric lineal chain of the hemicelluloses, which led to the lower effective activation energy. After the weaker bonds broke, the random scission on the lineal chain can be expected, which may cause the increase in the E_a value. However, the calculated E_a values within this zone are higher than the value for the single component of xylan (represents the hemicelluloses) usually analyzed in pyrolysis process (87.6 kJ/mol) [43]. The second process area spreads between $0.40 \leq \alpha \leq 0.80$, in which we have more or less stabilized E_a values around mean value $E_{a,\text{mean}} = 218.8$ kJ/mol, fig. 3(a). Also, the mean value of a pre-exponential factor was also calculated in this conversion range ($0.40 \leq \alpha \leq 0.80$) and amounts $(\log A)_{\text{mean}} = 19.135$ min^{-1}, fig. 3(b).

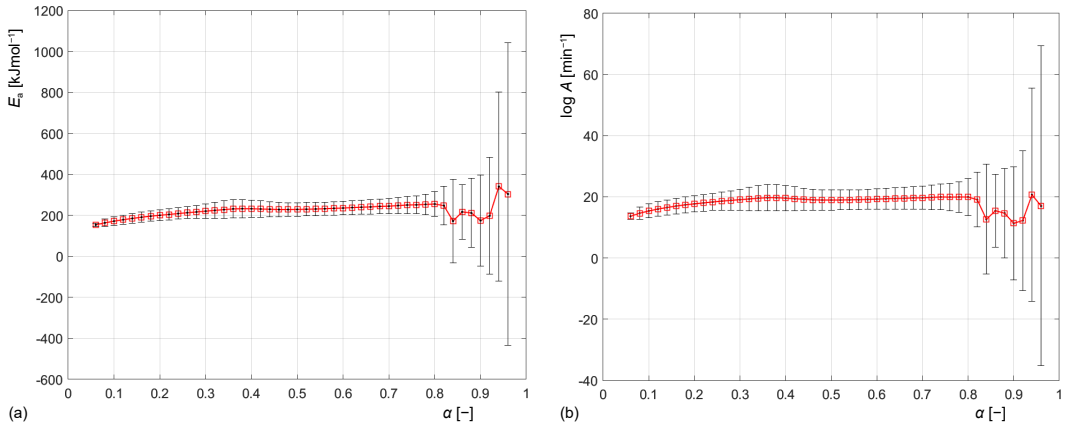

Figure 3. Activation energy E_a (a) and pre-exponential factor log$A$, (b) values in a function of conversion fractions α obtained by Friedman's differential method (the E_a and log$A$ error bars are also provided)

The indicated conversion range falls in the experimental temperature range where two mass loss rate peaks in DTG curves occur. Since that AKS has the high lignin content, this issue may lead to a tighter cross-link of three biomass constituents in the tested biomass sample. On the other hand, for cellulose decomposition in this reaction stage, the molecule initially pyrolyzed to active cellulose according to Briodo-Shafizadeh extended model, and this can lead to reducing of the degree of polymerization and the length of molecule chain. The active cellulose represents the intermediate product before further pyrolysis. This fact was validated from a certain increase of E_a value during transition from the first to the second reaction stage. In a considered conversion range ($0.40 \leq \alpha \leq 0.80$), the active cellulose continues to decompose with approximately constant effective activation energy, fig. 3. Finally, for $\alpha \geq 0.80$, the significant variation in E_a values can be observed, where this region corresponds to formation of the char contributed by secondary lignin decomposition reactions. Since that lignin is mainly composed of three kinds of benzene-propane, which was heavily cross-linked, these facts cause it to have

a very high thermal stability, requiring higher activation energy values as well. Likewise, a large amount of the char with reduced reaction reactivity can be formed in the actual process area, which may lead to increasing in the E_a value, and the introduction of certain instabilities towards the end of the pyrolysis. Consequently, the identified activation energy variation trend can be attributed to various functional groups in the macromolecular structure. Their chemical bonds break under different activation energies in the various pyrolysis temperature zones.

Determination of the most probable mechanism functions for decomposition reactions of biomass constituents during slow pyrolysis process

The most probable mechanism functions for thermal decomposition reactions of AKS constituents (marked as: S-1: Hemicelluloses, S-2: Cellulose, S-3: Lignin – the primary decomposition, S-4: Lignin – the secondary decomposition) are established by applying master plots method, through comparison of the experimental and theoretical $z(\alpha)$ master-plots. Reaction model plots are obtained from thirty six $g(\alpha)$ equations listed in [18]. Calculation of pre-exponential factor was performed in accordance with procedure described in sub-section *Friedman isoconversional differential method*. Figures 4(a)-4(d) shows the experimental $z(\alpha)$ plots ob-

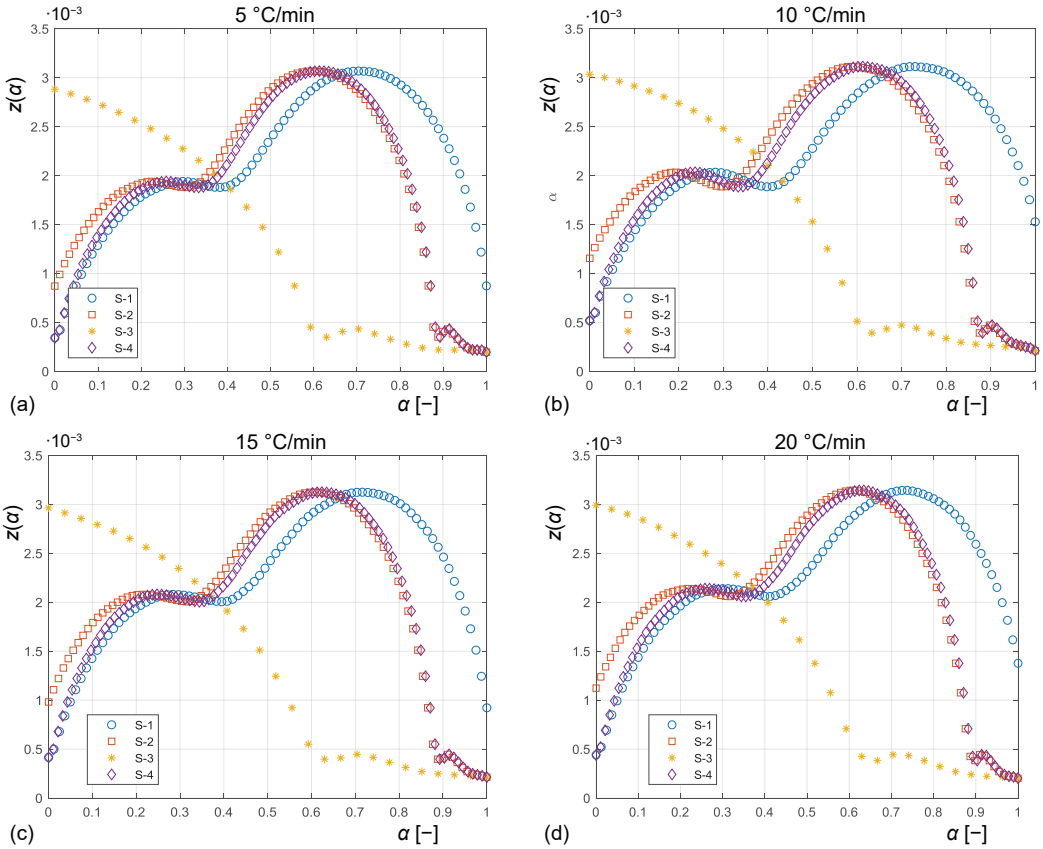

Figure 4. Experimental $z(\alpha) - \alpha$ plots for decomposition processes of S-1, S-2, S-3, and S-4 constituents during slow pyrolysis process of AKS at various heating rates: (a) 5 °C/min, (b) 10 °C/min, (c) 15 °C/min, and (d) 20 °C/min

tained at different heating rates (β = 5, 10, 15, and 20 °C per minute), for S-1, S-2, S-3, and S-4 decomposition reactions of the AKS slow pyrolysis.

From presented results in fig. 4, it can be observed that all $z(\alpha)$ plots for decomposition reactions related to S-1, S-2, S-3, and S-4 exhibit almost identical behavior in respect to changing of heating rate. Only the form of the $z(\alpha)$ function for the S-3 differs from the others, which indicated that the lignin primary decomposing reaction exhibits variety in kinetic behavior in respect to other decomposition reactions, where the rate progressively decreases until $\alpha \sim 0.64$, while simultaneously, the rates for the cellulose and secondary lignin decompositions reach the maximum values, fig. 4. The slight increase in the rate of the S-3 can be identified around conversion $\alpha \sim 0.70$, which roughly corresponds to the maximum value of the $z(\alpha)$ function for the hemicelluloses decomposition. It is obviously, that considering the shapes of the $z(\alpha)$ functions, it can be concluded that the reaction mechanisms are quite complex, especially for primary decomposition pathway related to lignin molecule. Therefore, the $z(\alpha)$ functions attributed to S-3 will be analyzed separately.

Firstly, the reaction mechanisms related to S-1, S-2, and S-4 decomposition processes were determined and results are shown in fig. 5. Considering all heating rates, for hemicelluloses and cellulose decomposition reactions, as well as for the secondary decomposition reaction of lignin, the order-based models F3 and F3/4 ($f(\alpha) = (1/2)(1 - \alpha)^3$ (F3 model) and $f(\alpha) = 4(1 - \alpha)^{3/4}$ (F3/4 model)) dominate, especially at lower conversions (up to approximately $\alpha \sim 0.35$) and at high conversion values ($\alpha \geq 0.90$). On the other hand, in a central and towards higher conversions, the rate-determining step was changed from order-based to nucleation/growth-based model, as 2-D Avrami-Erofeev (nucleation and subsequent growth) model ($f(\alpha) = 2(1 - \alpha)[-\ln(1 - \alpha)]^{1/2}$). For hemicelluloses decomposition, at lower conversions which was reflected in temperature range of 190-270 °C, the third-order (F3) reaction model governs the process, where dehydration and cleavage of the side chains of hemicelluloses occur, where the decarboxylation and decarbonylation reactions also take places. As temperature increases, and with transition into the higher conversion values, the fragmentation of other de-polymerized units takes primacy. Similar case stands for cellulose decomposition, where in the central and higher conversion ranges, the nucleation mechanism (A2) is reflected through the chain scission mechanism, indicating that the majority of pyrolysis reaction is dominated by the breakage of cellulosic polymeric bonds in a random manner (the obtained model can be relates to temperature-controlled nucleation and diffusion 2-D nuclei growth mechanism, where this is mostly closed to situation when the cellulose chains sufficiently fragmented, a grater fraction of scissions will produce the volatilization). From the two-step reaction model mechanism (involving F3 and A2 models) for hemicelluloses decomposition, we may expect that first stage can involve the competitive formation of volatiles and intermediate products, while second stage involves condensation and formation of bio-char and volatiles. Namely, the low molecular mass chains can probably act as centers for random nucleation and growth for the decomposition reaction. This is agreement with results shown in fig. 3, where E_a obtained is significantly lower than E_a of cellulose decomposition. Videlicet, the homogeneous un-branched structure of cellulose accounted for its well-defined decomposition temperature range and the higher E_a while the branched units on the hemicelluloses structure gave a lower E_a, and hence more readily to be broken down at a lower temperature range. So, the considering hemicelluloses and cellulose pyrolysis reactions, many authors performed kinetic analysis related to these pseudo-components using first order reaction, the present study indicates that first order mechanism (which corresponds to random nucleation with one nucleus in the individual particle) is not suitable for hemicelluloses decomposition due to the large deviation existed throughout the process as

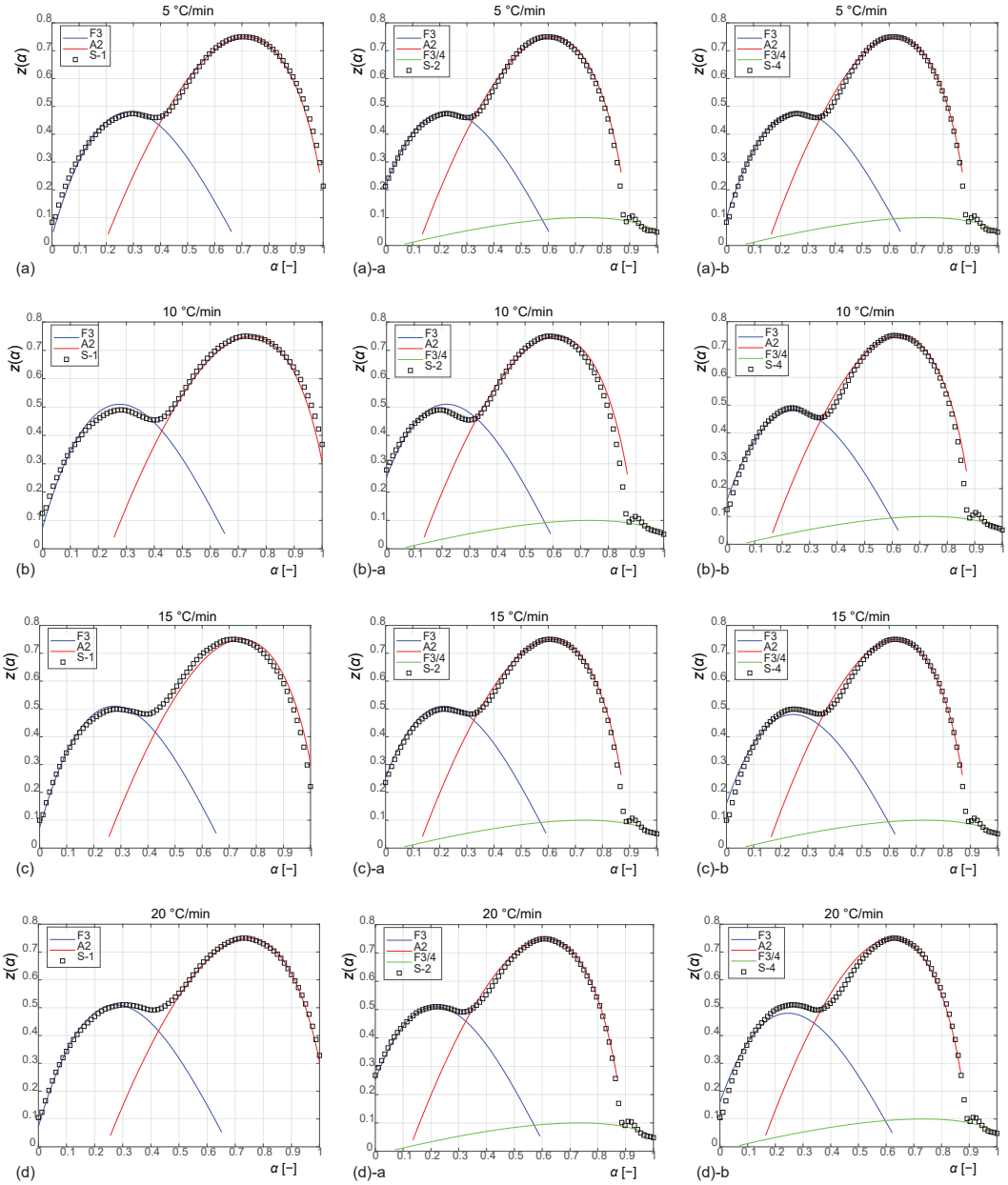

Figure 5. The $z(\alpha)$ profiles for S-1, S-2, and S-4 constituents of AKS pyrolysis at various heating rates in the combined reaction mechanism model (□ – experimental; colored full lines are related to theoretical reaction models)

shown in fig. 5. This conclusion was in agreement with result reports published by Hu *et al.* [44] and Bar-Gadda [45]. However, for lignin secondary decomposition reaction pathway in conversion range of approximately $\Delta\alpha = 0.35 - 0.89/0.90$, the 2-D nucleation/growth reaction model (especially at the higher temperatures) is valid, and in agreement with results reported in [46]. Since the lignin contains the various oxygen functional groups which have different

thermal stability, the scission reactions may occur at different temperatures in a fairly large conversion range. In addition, the lignin with the complex and rigid cross-linked structure requires more energy than hemicelluloses for pyrolysis to destroy the phenolic structure. It can be supposed that the main stage of lignin decomposition may involve thermal cracking of all linkages and conversion of methoxy substituents. This reaction is probably controlled through reaction order mechanism, with order of reaction higher than unity ($n > 1$), and due to disorder process mechanism [47].

Generally, for all observed cases, the high reaction order (F3), fig. 5, can represents the combination of diffusion and power-law mechanism. Due to its complex composition and structure, lignin decomposition is strongly influenced by its nature, the reaction temperature and decomposing atmosphere, with considerable effect on the conversion and product yields, as well as on the physical properties and quality of pyrolysis products. However, it should be noted, that for both, the cellulose and lignin secondary decomposition reactions, which occurs at the high conversions, the reaction order model with $n \sim 0.75$ (F3/4) exists, fig. 5. In this respect, the higher activation energy means a slower reaction affecting on the char formation, where the reaction order drops below the unity. So, the cellulose and lignin decomposition reactions at the elevated temperatures contribute to a large extent to the formation of char in the pyrolysis process.

It should be emphasized that the existence of alkali metals in the ash can catalyzes formation of the char during pyrolysis, which has a direct correlation with chemical reactivity of the pyrolysis process of the AKS. Namely, the char alone, and char-supported metals are potential catalysts for the tar production during and even after biomass gasification. In the slow pyrolysis process, the lower heating rates and longer residence times favor the secondary cracking of vapors and thus, may lead to the higher bio-char yield.

Figures 6(a)-6(d) shows the comparison between experimental and the model master plots [$z(\alpha) - \alpha$] estimated for the primary decomposition reaction mechanism, attached to lignin constituent (S-3) at various heating rates.

It can be observed that the primary lignin decomposition stage involves the variety of the reaction mechanisms. So, the rate of the process changes more intensively depending on the apparent change in the type of reaction mechanism as well as conversion values into products of the pyrolysis. Independently on the heating rate applied, with progressive increasing of temperature and conversion (up to $\alpha \sim 0.62$), the process at this stage starts with cleavages of the β–β and C–C linkages between lignin monomeric units, where the recombination of the formed radicals leads to guaiacyl and syringyl compounds [48]. However, guaiacols and syringols are intermediate decomposition products and their amount decreases with an increasing of pyrolysis temperature.

This is accompanied by the decrease in the reaction rate, where transformation is followed by non-integer reaction order as F3/2 [$f(\alpha) = 2(1 - \alpha)^{3/2}$], fig. 6. After that, the slight increase of the process rate can be identified, and in further progression, the 2-D diffusion (G7) ($f(\alpha) = 4\{(1 - \alpha)[1 - (1 - \alpha)]^{1/2}\}^{1/2}$) and nucleation (P2/3) [$f(\alpha) = (2/3)\alpha^{-1/2}$] phenomena occur, fig. 6. Realized events in this case indicate that the primary lignin decomposition step represents the slowest step in entire pyrolysis process of AKS where in a great manner contributes kinetically characterized reaction, fig. 6. In the conversion range of $\Delta\alpha \sim 0.62$-0.80, the decomposition mechanism refers to the diffusion in 2-D, where this mechanism may suggest grater decomposition of lignin at higher temperatures, leading to the higher volatility rate from this constituent. In an addition, the char pore lattice defects can be considered as significant factor since these defects promote reactivity and the diffusion of the material. At the very end of this stage (above conversion, $\alpha \sim 0.90$), fig. 6, the nucleation mechanism

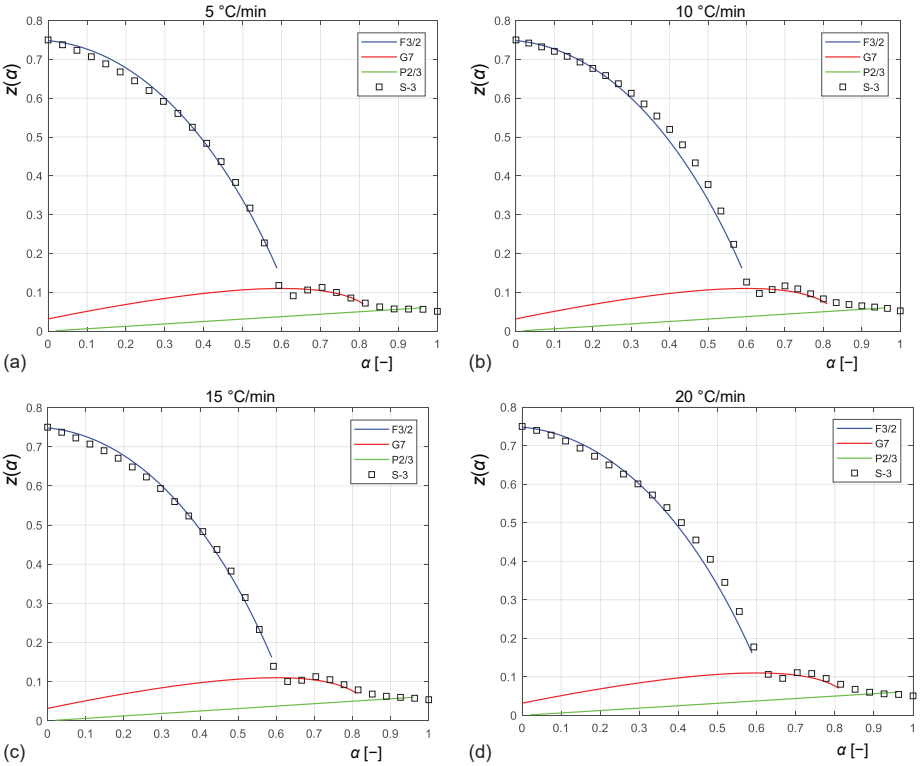

Figure 6. The $z(\alpha)$ profiles for S-3 related to lignin primary decomposition reaction mechanism in AKS pyrolysis, which includes combined reaction mechanism model at various heating rates (□ – experimental; colored full lines are related to theoretical reaction models)

takes place. At that moment, the nucleation reaction pathway can indicate on the presence of the active zones more chemically liable to the thermal decomposition. Overview of all existing pyrolysis rate equations formed from the estimated reaction mechanism models for every considered constituent of the AKS sample is presented in tab. 3.

The established kinetic parameters and models presented in this work were confirmed through four-step (parallel) kinetic modeling of AKS slow pyrolysis, which was presented in our previously published study [19].

Conclusions

In this study, the kinetic pyrolysis characteristics of AKS samples are analyzed using the combined isoconversional (model-free) and master-plots analyses. The results report opportunity to separate pyrolysis reactions of hemicelluloses, cellulose, primary and secondary lignin as main constituents in the investigated waste biomass. It was found that the decomposition reactions of hemicelluloses and cellulose correspond to the order-based reaction mechanisms and the random scission mechanism. The lignin decomposition is a more complex, which proceeds, through the primary and secondary reaction pathways. It was found that decomposition of lignin involves the combination of the effects of the non-integer order-based, the 2-D diffusion as well as nucleation mechanisms. It was assumed that the formation of the aromatic hydrocarbons from lignin constituent is the exceptionally high, due to the vigorous

Table 3. The rate-law equations that exist during the complex process of slow pyrolysis of AKS sample, including decomposition behavior of individually separated biomass constituents, marked by S-1, S-2, S-3, and S-4, respectively, (in a given table, the differential form of reaction mechanism functions, $f(\alpha)$, are presented)

S1	F3	$\frac{\mathrm{d}\alpha_{11}}{\mathrm{d}T}=\frac{A_{11}}{\beta}\exp\left(-\frac{E_{a,11}}{\mathrm{R}T}\right)\frac{1}{2}\left(1-\alpha_{11}\right)^{3}$
	A2	$\frac{\mathrm{d}\alpha_{12}}{\mathrm{d}T}=\frac{A_{12}}{\beta}\exp\left(-\frac{E_{a,12}}{\mathrm{R}T}\right)2\left(1-\alpha_{12}\right)\left[-\ln\left(1-\alpha_{12}\right)\right]^{\frac{1}{2}}$
S2	F3	$\frac{\mathrm{d}\alpha_{21}}{\mathrm{d}T}=\frac{A_{21}}{\beta}\exp\left(-\frac{E_{a,21}}{\mathrm{R}T}\right)\frac{1}{2}\left(1-\alpha_{21}\right)^{3}$
	A2	$\frac{\mathrm{d}\alpha_{22}}{\mathrm{d}T}=\frac{A_{22}}{\beta}\exp\left(-\frac{E_{a,22}}{\mathrm{R}T}\right)2\left(1-\alpha_{22}\right)\left[-\ln\left(1-\alpha_{22}\right)\right]^{\frac{1}{2}}$
	F3/4	$\frac{\mathrm{d}\alpha_{23}}{\mathrm{d}T}=\frac{A_{23}}{\beta}\exp\left(-\frac{E_{a,23}}{\mathrm{R}T}\right)4\left(1-\alpha_{23}\right)^{\frac{3}{4}}$
S3	F3/2	$\frac{\mathrm{d}\alpha_{31}}{\mathrm{d}T}=\frac{A_{31}}{\beta}\exp\left(-\frac{E_{a,31}}{\mathrm{R}T}\right)2\left(1-\alpha_{31}\right)^{\frac{3}{2}}$
	G7	$\frac{\mathrm{d}\alpha_{32}}{\mathrm{d}T}=\frac{A_{32}}{\beta}\exp\left(-\frac{E_{a,32}}{\mathrm{R}T}\right)4\left\{\left(1-\alpha_{32}\right)\left[1-\left(1-\alpha_{32}\right)^{\frac{1}{2}}\right]\right\}^{\frac{1}{2}}$
	P2/3	$\frac{\mathrm{d}\alpha_{33}}{\mathrm{d}T}=\frac{A_{33}}{\beta}\exp\left(-\frac{E_{a,33}}{\mathrm{R}T}\right)\frac{2}{3}\alpha^{-\frac{1}{2}}$
S4	F3	$\frac{\mathrm{d}\alpha_{41}}{\mathrm{d}T}=\frac{A_{41}}{\beta}\exp\left(-\frac{E_{a,41}}{\mathrm{R}T}\right)\frac{1}{2}\left(1-\alpha_{41}\right)^{3}$
	A2	$\frac{\mathrm{d}\alpha_{42}}{\mathrm{d}T}=\frac{A_{42}}{\beta}\exp\left(-\frac{E_{a,42}}{\mathrm{R}T}\right)2\left(1-\alpha_{42}\right)\left[-ln\left(1-\alpha_{42}\right)\right]^{\frac{1}{2}}$
	F3/4	$\frac{\mathrm{d}\alpha_{43}}{\mathrm{d}T}=\frac{A_{43}}{\beta}\exp\left(-\frac{E_{a,43}}{\mathrm{R}T}\right)4\left(1-\alpha_{43}\right)^{\frac{3}{4}}$

dehydroxylation of the phenol-type compounds enhanced by the inorganic impurities located inside the AKS samples. It can be assumed that accumulation/growth of polycyclic aromatic hydrocarbons (PAH) can be expected in solid residue (bio-char), since that PAH with larger molecular weights exhibit high stability (their bond dissociation energies spread up to 1000 kJ/mol) at high operational temperatures. Since that in this work, the secondary lignin cracking reactions take place, the more volatiles liberation and forming of aromatics amorphous carbon structures should be expected to occur.

The detailed explanation of the mechanistic scheme related to thermal decomposition of every biomass constituent was exposed in this study. The complete list of rate-law equations that exist during slow pyrolysis of AKS sample was also provided.

Based on lab-scale thermochemical conversion experiments performed in this work, it can be concluded that waste biomass (AKS) has a good potential for production of bio-char (from dynamic TA measurements the averaged bio-char yield is about 27%) and chemicals (tar). However, the bio-char yield greatly depends on the adaption of pyrolysis type. Slow pyrolysis performed at longer residence time and at a moderate temperature (between 350 °C and 550 °C) results in higher yield of biochar, than fast pyrolysis or gasification. Therefore, the results of this study may serve as a favorable platform for future research related to fast pyrolysis and torrefaction experiments, in order to obtain high yields of liquid (bio-oil) and solid (bio-char) products.

Acknowledgment

Authors would like to acknowledge financial support of Ministry of Education, Science and Technological Development of the Republic of Serbia.

Nomenclature

A – preexponential factor
d_p – hole size
$E_{a,\,\mathrm{mean}}$ – mean activation energy
HHV – higher heating value, [kJkg^{-1}]
LHV – lower heating value, [kJkg^{-1}]
m_f – final biomass sample
m_o – initial biomass sample
m_T – current biomass sample at arbitrary T and at the time t
n – reaction order
T – temperature, [K]
t – time, [min]
VM – volatile matter, [%]

Greek symbols

α – conversion, [–]
β – heating rate, [°Cmin^{-1}]

Acronyms

AKS – apricot kernel shell
DTG – derivative thermogravimetry
FC – fixed carbon
TA – thermoanalytical
TGA – thermogravimetric analysis

References

[1] Gagliano, A., *et al.*, A Robust Numerical Model for Characterizing the Syngas Composition in a Downdraft Gasification Process, *Comp. Rendus Chem*., *19* (2016), 4, pp. 441-449
[2] Nicoletti, G., *et al.*, On the Generalized Concept of Entropy for Physical, Extraphysical and Chemical Processes, *Int. J. Heat Technol., 34* (2016), 1, pp. S21-S28
[3] Mansaray, K. G., Ghaly, A. E., Kinetic Analyses of Biomass Pyrolysis Using the Distributed Energy of Activation Model, *Biomass & Bioenergy, 17* (1999), 1, pp. 19-31
[4] Vuthaluru, H. B., Investigations into the Pyrolytic Behavior of Coal/Biomass Blends Using Thermogravimetric Analysis, *Bioresour. Technol., 92* (2004), 2, pp.187-195
[5] Sonobe, T., Worasuwannarak, N., Kinetic Analyses of Biomass Pyrolysis Using the Distributed Energy of Activation Model, *Fuel, 87* (2008), 3, pp. 414-421
[6] Seo, D. K., *et al.*, Study of the Pyrolysis of Biomass Using Thermo-Gravimetric Analysis (TGA) and Concentration Measurements of the Evolved Species, *J. Anal. Appl. Pyrol., 89* (2010), 1, pp. 66-73
[7] Saddawi, A., *et al.*, Kinetics of the Thermal Decomposition of Biomass, *Energy Fuels, 24* (2010), 2, pp. 1274-1282
[8] Vyazovkin, S., Wight, C. A., Isothermal and Non-Isothermal Kinetics of Thermally Stimulated Reactions of Solids, *Int. Rev. Phys. Chem., 17* (1998), 3, pp. 407-433
[9] White, J. E., *et al.*, Biomass Pyrolysis Kinetics: A Comparative Critical Review with Relevant Agricultural Residue Case Studies, *J. Anal. Appl. Pyrol., 91* (2011), 1, pp. 1-33
[10] Cai, J., *et al.*, Logistic Regression Model for Isoconversional Kinetic Analysis of Cellulose Pyrolysis, *Energy Fuels, 22* (2008), 2, pp. 867-870
[11] Friedman, H. L., Kinetics of Thermal Degradation of Char-Forming Plastics from Thermogravimetry, Application to a Phenolic Plastic*, J. Polym. Sci. C Polym. Symp., 6* (1964), 1, pp. 183-195
[12] Yao, F., *et al.*, Thermal Decomposition Kinetics of Natural Fibers: Energy of Activation with Dynamic Thermogravimetric Analysis, *Polym. Degrad. Stab., 93* (2008), 1, pp. 90-98

[13] Gotor, F. J., *et al.*, Kinetic Analysis of Solid-State Reactions: The Universality of Master Plots for Analyzing Isothermal and Nonisothermal Experiments, *J. Phys. Chem., A 104* (2000), 46, pp. 10777-10782
[14] Šoštarić, T., *et al.*, Application of Apricot Stone Waste from Fruit Processing Industry in Environmental Cleanup: Copper Biosorption Study., *Fruits, 70* (2015), 5, pp. 271-280
[15] ***, EN ISO 14780:2017, Solid Biofuels – Sample Preparation, European Committee for Standardization (CEN), 2017, Brussels, Belgium, 2017
[16] ***, EN ISO 17225-1:2014, Solid Bbiofuels – Fuel Specifications and Classes – Part 1: General Requirements, European Committee for Standardization (CEN), 2014, Brussels, Belgium, 2014
[17] Capart, R., *et al.*, Assessment of Various Kinetic Models for the Pyrolysis of a Microgranular Cellulose, *Thermochim. Acta, 417* (2004), 1, pp. 79-89
[18] Sronsri, C., *et al.*, Thermal Decomposition Kinetics of $Mn_{0.9}Co_{0.1}HPO_4 \cdot 3H_2O$ Using Experimental-Model Comparative and Thermodynamic Studies, *J. Therm. Anal. Calorim., 127* (2017), 3, pp. 1983-1994
[19] Manić, N., *et al.*, Apricot Kernel Shells Pyrolysis Controlled by Non-Isothermal Simultaneous Thermal Analysis (STA), *J. Therm. Anal. Calorim.* On-line first, https://doi.org/10.1007/s10973-020-09307-5, 2020
[20] Ma, H., *et al.*, Kinetic Analysis of the Pyrolysis of Apricot Stone and its Main Components *via* Distributed Activation Energy Model, *Bioresources, 15* (2020), 1, pp. 1187-1204
[21] ***, EN ISO 18125:2017, Solid Biofuels – Determination of Calorific Value, European Committee for Standardization (CEN), Brussels, Belgium, 2017
[22] Savova, D., *et al.*, Production of Carbon Adsorbents from Biomass and Biomass Products, In: 1st World Conference on Biomass for Energy and Industry, *Proceedings,* Conference Held in Sevilla, Spain, 2000, S. Kyritsis, A. A. C. M. Beenackers, P. Helm, A. Grassi, D. Chiaramonti (Editors), James & James (Science Publishers) Ltd., Printed in the UK by MPG Books Ltd., ISBN 1 902916 158, 2001, pp. 1040-1044
[23] Janković, B., *et al.*, Physico-Chemical Characterization of Carbonized Apricot Kernel Shell as Precursor for Activated Carbon Preparation in Clean Technology Utilization, *J. Cleaner Prod., 236* (2019), Nov., pp. 117614
[24] Bota, A., Laszlo, K., Preparation of Activated Carbon from Apricot Pits, *Period. Polytech. Ser. Chem. Eng., 44* (1997), 1, pp. 19-24
[25] Soleimani, M., Kaghazchi, T., Agricultural Waste Conversion to Activated Carbon by Chemical Activation with Phosphoric Acid, *Chem. Eng. Technol., 30* (2007), 5, pp. 649-654
[26] Razvigorova, M., *et al.*, On the Composition of Volatiles Evolved During the Production of Carbon Adsorbents from Vegetable Wastes, *Fuel, 73* (1994), 11, pp. 1718-1722
[27] Cagnon, B., *et al.*, Contributions of Hemicellulose, Cellulose and Lignin to the Mass and the Porous Properties of Chars and Steam Activated Carbons from Various Lignocellulosic Precursors, *Bioresour. Technol., 100* (2009), 1, pp. 292-298
[28] Allouch, D., *et al.*, Characterization of Components Isolated from Algerian Apricot Shells (*Prunus Armeniaca* L.), *Cellulose Chem. Technol., 53* (2019), 9-10, pp. 851-859
[29] Petrov, N., *et al.*, Preparation of Activated Carbons from Cherry Stones, Apricot Stones and Grape Seeds for Removal of Metal Ions from Water, *Proceedings*, 2nd Olle Indstorm Symposium on Renewable Energy-Bioenergy, At KTH, Stockholm, Sweden, 1999, pp. 46-50
[30] Black, J., Cost and Performance Baseline for Fossil Energy Plants Volume 1: Bituminous Coal and Natural Gas to Electricity, National Energy Technology Laboratory: Washington DC, USA, 2010
[31] Silva, J. E., *et al.*, Energy Potential and Thermogravimetric Study of Pyrolysis Kinetics of Biomass Wastes, *J. Therm. Anal. Calorim., 137* (2019), Feb., pp. 1635-1643
[32] Zhang, L., *et al.*, Co-Pyrolysis of Biomass and Coal in a Free Fall Reactor, *Fuel, 86* (2007), 3, pp. 353-359
[33] Van Krevelen, D. W., *Coal: Typology-Physics-Chemistry-Constitution*, Elsevier Science, Amsterdam, The Netherlands, 1993
[34] Quan, C., *et al.*, Pyrolysis of Biomass Components in a TGA and Fixed-Bed Reactor: Thermochemical Behaviors, Kinetics, and Product Characterization, *J. Anal. Appl. Pyrol., 121* (2016), Sept., pp. 84-92
[35] Fox, S. C., McDonald, A G., Chemical and Thermal Characterization of Three Industrial Lignins and Their Corresponding Lignin Esters, *Bioresources, 5* (2010), 2, pp. 990-1009
[36] Pandey, M. P., Kim, C. S., Lignin Depolymerization and Conversion: A Review of Thermochemical Methods, *Chem. Eng. Technol., 34* (2011), 1, pp. 29-41
[37] Lazaridis, P. A., *et al.*, Catalytic Fast Pyrolysis of Kraft Lignin with Conventional, Mesoporous and Nanosized ZSM-5 Zeolite for the Production of Alkyl-Phenols and Aromatics, *Front. Chem., 6* (2018), July, pp. 295-315

[38] Jiang, G., *et al.*, Effect of the Temperature on the Composition of Lignin Pyrolysis Products, *Energy Fuels, 24* (2010), 8, pp. 4470-4475
[39] Ounas, A., *et al.*, Pyrolysis of Olive Residue and Sugar Cane Bagasse: Non-Isothermal Thermogravimetric Kinetic Analysis, *Bioresour. Technol., 102* (2011), 24, pp. 11234-11238
[40] Ozveren, U., Ozdogan, Z. S., Investigation of the Slow Pyrolysis Kinetics of Olive Oil Pomace Using Thermo-Gravimetric Analysis Coupled with Mass Spectrometry, *Biomass & Bioenergy, 58* (2013), Nov., pp. 168-179
[41] Chaiwat, W., *et al.*, Analysis of Cross-Linking Behavior During Pyrolysis of Cellulose for Elucidating Reaction Pathway, *Energy Fuels, 23* (2009), 12, pp. 5765-5772
[42] Agarwal, V., *et al.*, Ab Initio Dynamics of Cellulose Pyrolysis: Nascent Decomposition Pathways at 327 and 600 °C, *J. Am. Chem. Soc., 134* (2012), 36, pp. 14958-14972
[43] Yang, H. P., *et al.*, Thermogravimetric-Analysis-Fourier Transform Infrared Analysis of Palm Oil Waste Pyrolysis, *Energy Fuels, 18* (2004), 6, pp.1814-1821
[44] Hu, S., *et al.*, Kinetic Study of Chinese Biomass Slow Pyrolysis: Comparison of Different Kinetic Models, *Fuel, 86* (2007), 17-18, pp. 2778-2788
[45] Bar-Gadda, R., The Kinetics of Xylan Pyrolysis, *Thermochim. Acta., 42* (1980), 2, pp. 153-163
[46] Volker, S., Rieckmann, T., The Potential of Multivariate Regression in Determining Formal Kinetics of Biomass, in: *Progress in Thermochemical Biomass Conversion*. Vol. 1, (Ed. A. V. Bridgwater), Blackwell Science Ltd., London, UK, 2001, pp. 1076-1091
[47] Manya, J. J., *et al.*, Kinetics of Biomass Pyrolysis: A Reformulated Three-Parallel-Reactions Model, *Ind. Eng. Chem. Res., 42* (2003), 3, pp. 434-441
[48] Graham, G., Mattila, T., High Energy Degradation, in: *Lignin – Occurrence, Formation, Structures and Reactions*, (Ed. K. V. Sarkanen), Ludwig CH, Wiley, New York, USA, 1971, pp. 575-578

Paper submitted: February 13, 2020
Paper revised: May 1, 2020
Paper accepted: May 1, 2020